

Search for the decay $\mu^+ \rightarrow e^+e^-e^{+\ast}$

Roman Gredig^{1,†}

(For the Mu3e Collaboration)[‡]

¹*University of Zurich*

(Dated: April 15, 2016)

Abstract

Mu3e is a proposed experiment to be built at the Paul Scherrer Institute searching for the charged lepton flavor violating decay $\mu^+ \rightarrow e^+e^-e^+$ with a sensitivity of $\mathcal{B} < 10^{-16}$, four orders of magnitudes lower than its predecessor SINDRUM [1]. The following proceeding gives an overview over the experiment and the current R&D efforts in building a silicon pixel tracker and time hodoscope consisting of scintillating fibers and tiles. The detector components and a read-out strategy for the whole experiment are described.

INTRODUCTION

In the standard model lepton flavor is conserved at tree level. The observation of neutrino oscillations by experiments such as SuperKamiokande [2], SNO [3], and KamLAND [4] is, however, a direct proof of lepton flavor violation (LFV). Charged LFV (CLFV) would lead to $\mu \rightarrow e$ and $\tau \rightarrow \mu$ transitions without neutrinos in the final state. In the standard model CLFV can only be induced by neutrino mixing (see Fig. 1 for the decay of interest here) but such processes are highly suppressed by the tiny neutrino masses. The resulting branching ratios are below 10^{-50} , way beyond the experimental sensitivity. The observation of CLFV would therefore directly signal physics beyond the standard model. Two examples are shown in Fig. 1 as well. Muon number violation has already been investigated in different channels (see Tab. I). When these processes would be observed their relative strengths would guide the attempts to identify the underlying mechanism. A new $\mu^+ \rightarrow e^+e^-e^+$ search has been proposed at the Paul Scherrer Institute (PSI) aiming at a hitherto unreached sensitivity down to $\mathcal{B} < 10^{-16}$ [5], four orders of magnitude more sensitive than reached by its 27 years old predecessor SINDRUM.

TABLE I: Experimental upper limits on the branching ratios B of LFV muon decays

Decay channel	Experiment	\mathcal{B} upper limit	Ref.
$\mu \rightarrow e\gamma$	MEGA	$1.2 \cdot 10^{-11}$	[6]
	MEG	$5.7 \cdot 10^{-13}$	[7]
$\mu \rightarrow eee$	SINDRUM	$1.0 \cdot 10^{-12}$	[1]
$\mu^- \text{Au} \rightarrow e^- \text{Au}$	SINDRUM II	$7 \cdot 10^{-13}$	[8]

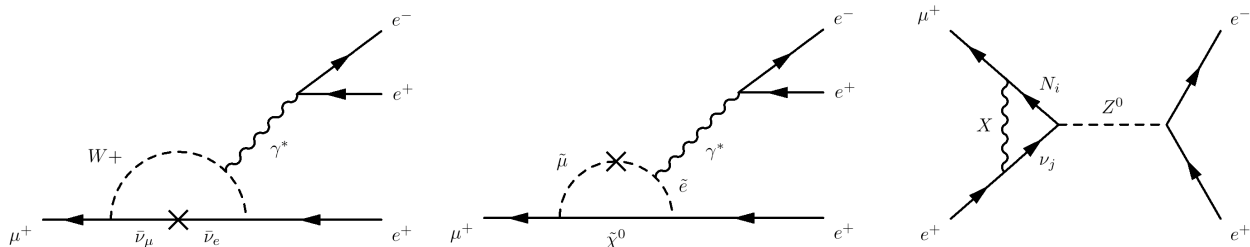


FIG. 1: Possible $\mu^+ \rightarrow e^+e^-e^+$ mechanisms. From the left: neutrino mixing allowed within the standard model, a supersymmetric contribution, and a penguin diagram in the little Higgs model.

DESIGN OF THE MU3E EXPERIMENT

A signal event in Mu3e are two positrons and one electron with common vertex, a vanishing sum of their momenta $\Sigma \vec{p}_i = 0$ and the muon mass as the total energy. The main challenge is the background suppression. An excellent momentum resolution of less than $0.5 \text{ MeV}/c$ is needed to identify the internal conversion background $\mu \rightarrow eee\nu\nu$ with a branching ratio $\mathcal{B} = 3.4 \cdot 10^{-5}$. In addition the combinatorial background needs to be suppressed by an excellent vertex locator, timing and momentum measurement.

The electron momenta are intended to be measured in a 1 T homogeneous magnetic field with silicon pixel detectors. Additional scintillating timing detectors are needed to suppress combinatorial background. The low momenta of the electrons ($p < 53 \text{ MeV}/c$) demand the reduction of the material in the active area to a minimum. Therefore the detector will be operated in a gaseous helium atmosphere. There will be a helium flow velocity of about 3 m s^{-1} to cool active components, as for example the silicon pixel sensors [9]. The readout FPGAs and timing detectors will be cooled by an additional liquid helium cooling system being outside the active area.

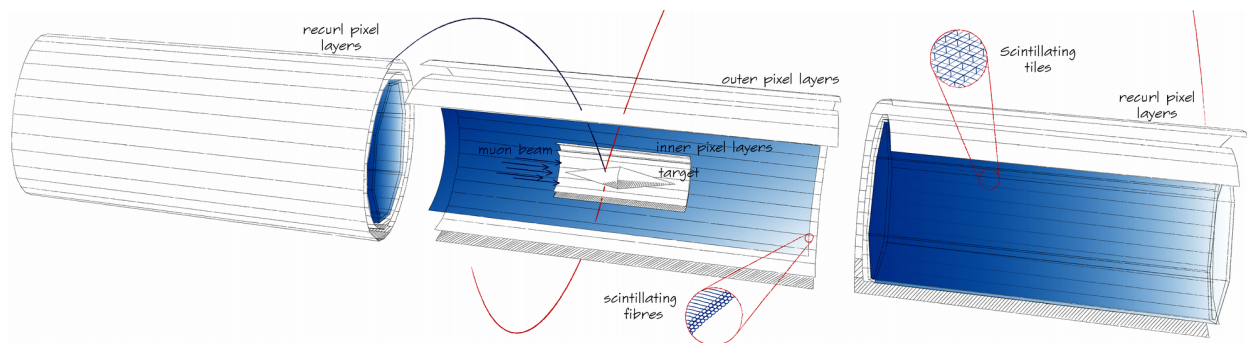


FIG. 2: Schematic of the central part of the Mu3e detector. The final detector consists of two more stations that are identical to the two stations on the side. Each station has a diameter of 17 cm and a length of 36 cm. The overall length of the final detector will be about 2 m.

A schematic of the experiment is shown in Fig. 2. The muons are stopped in a hollow double cone target in the middle of the detector. The target ensures a spread of the muon vertices to reduce the combinatorial background. The decay electrons propagate in a 1 T homogenous magnetic field. They pass the first two silicon pixel layers close to the target to identify the vertex and a second pair of pixel layers to specify the momentum. The momentum resolution precision depends in first order on the multiple scattering angle θ and the lever-arm Ω in a magnetic field to

$$\frac{\sigma_p}{p} \propto \frac{\theta_{MS}}{\Omega}. \quad (1)$$

A high lever arm by placing tracking stations at a large radius would increase the momentum resolution but also decrease the momentum acceptance. Therefore the electrons, after passing the second pair of trackers, propagate in the magnetic field until they curl back where they pass another pair of pixel layers. These layers are provided by two stations on each side of the central station. The momentum measurement with the recurling electrons

provides a momentum resolution of $0.5 \text{ MeV } c^{-1}$ while still having a wide momentum acceptance. Measuring the momentum with particles recurling close to an angle of π cancels out the error in momentum caused by multiple scattering at first order (Fig. 3).

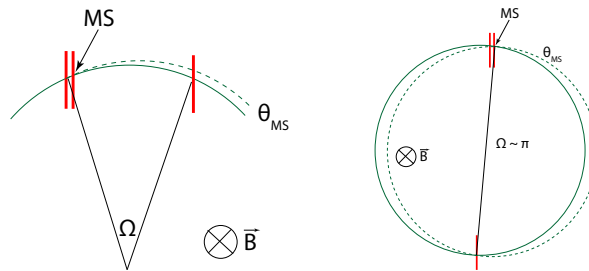


FIG. 3: Multiple scattering seen in the detector plane with the lever arm angle Ω (left) and the multiple scattering for a recurling particle (right).

Separating the decays requires additional timing detectors. The central part is extended with three layers of $250 \mu\text{m}$ thick scintillating fibers read out by silicon photomultipliers at both fibre ends. The outer stations have scintillation tiles close to the pixel sensors. The fibers require to have a time resolution below 1 ns while the tiles resolution needs to be better than 100 ps .

The modular structure allows to build and run the detector at different stages. In a first phase the detector will only consist of the central module and one recurl station at each side as shown in Fig. 2. The planned sensitivity goal is set at $\mathcal{B}(\mu \rightarrow eee) < 10^{-15}$. In a second phase each side of the detector will be expanded with an additional recurl station that allows to detect all recurling particles that are within the acceptance given by the central module. The second phase sensitivity goal is set at $\mathcal{B}(\mu \rightarrow eee) < 10^{-16}$. The feasibility of a beam intensity of $\sim 10^8$ muons per second has already been shown at PSI at the πE5 beamline fulfilling the requirements for the first phase. A new beamline providing $\sim 10^9$ muons per second as needed for the second phase is currently under investigation at PSI.

MONOLITHIC ACTIVE PIXEL SENSORS

With the Mu3e experiment a new pixel sensor technology will be introduced, the High Voltage Monolithic Active Pixel Sensor (HV-MAPS) [10]. The sensor consists of a depleted area biased with $\sim 70 \text{ V}$ enabling a fast $\mathcal{O}(1 \text{ ns})$ charge collection via drift. The digitization and the serial driver to write out the (zero suppressed) data are part of the chip itself. The data written consists of the hit pixel address and a time-stamp.

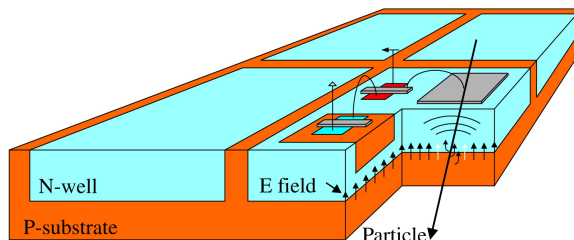


FIG. 4: Schematic view of HV-MAPS [10]

Each sensor-module consists of an active area of $2 \times 2 \text{ cm}^2$ with an individual pixel size of $80 \times 80 \mu\text{m}^2$. The sensor thickness will be less than $50 \mu\text{m}$. Together with a Kapton support structure of $25 \mu\text{m}$ and flexprint cables that provide supply voltage and readout data lines, the thickness will be about 1 permille radiation length X_0 . In the current prototype design (version 7) the chip already reaches a time resolution of $\sim 17 \text{ ns}$ with a pixel efficiency of $> 99 \%$. Using such small pixels the tracking resolution is dominated by multiple scattering and a smaller pixel size would not help improving the detector resolution. The HV-MAPS are produced by commercial CMOS technology leading to a rather cheap production technology as widely used in industrial processes. The current pixel R&D achieved a working chip at a still smaller active area of $2.9 \times 3.2 \text{ mm}^2$. A new series of chips is under commissioning that will have the proposed size of the active area.

TIME OF FLIGHT SYSTEM

Scintillating Fibres

The fibers at the central station of the detector will be placed close to the outer pixel layers. The photons generated in the fibers will be guided within the fibers out of the active area where they are detected at the fiber ends only. Each fiber has a diameter of $250 \mu\text{m}$ and a length of 30 cm . Three layers of fibers are glued together to 16 mm wide ribbons (see Fig. 5). These ribbons are placed close to the outer layers of the silicon pixel sensors. The scintillation light will be read out by silicon photomultipliers (SiPMs). Two readout schemes are currently discussed. Either an individual readout where each fiber is read out by an individual SiPM or a column wise readout where the fibre modules can be directly attached to 16 mm wide SiPM arrays. The SiPM technology allows to place up to about 4500 SiPMs dense enough to fit into the detector and they can be operated in a 1 T magnetic field environment.

Currently round and squared double cladding fibers are under investigation. First prototype R&D shows that squared fibers provide a time resolution better than 500 ps whereas the round fibers perform with about 1.5 ns . Several full size ribbons made with round shaped fibers have already been built and a tool for mass production has been developed.

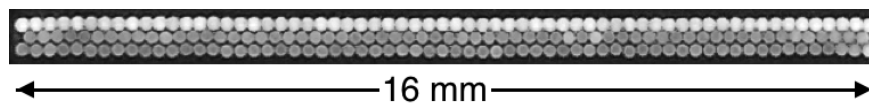


FIG. 5: Front view of a fibre ribbon prototype

Scintillating Tiles

The plastic scintillating tiles of the outer detector modules have a size of about $1 \times 1 \times 1 \text{ cm}^3$. Each station of the detector will have 3360 tiles where all are read out individually by a single SiPM. Thirtytwo tiles will be combined to submodules as shown in Fig. 6 left with two 4×4 tile arrays. Fifteen submodules together form a module of 480 channels. These modules are placed around the beam pipe (see Fig. 6, right) covering one station. For the

tiles the required time resolution better than 100 ps has already been proved by several test-beam measurements [11].

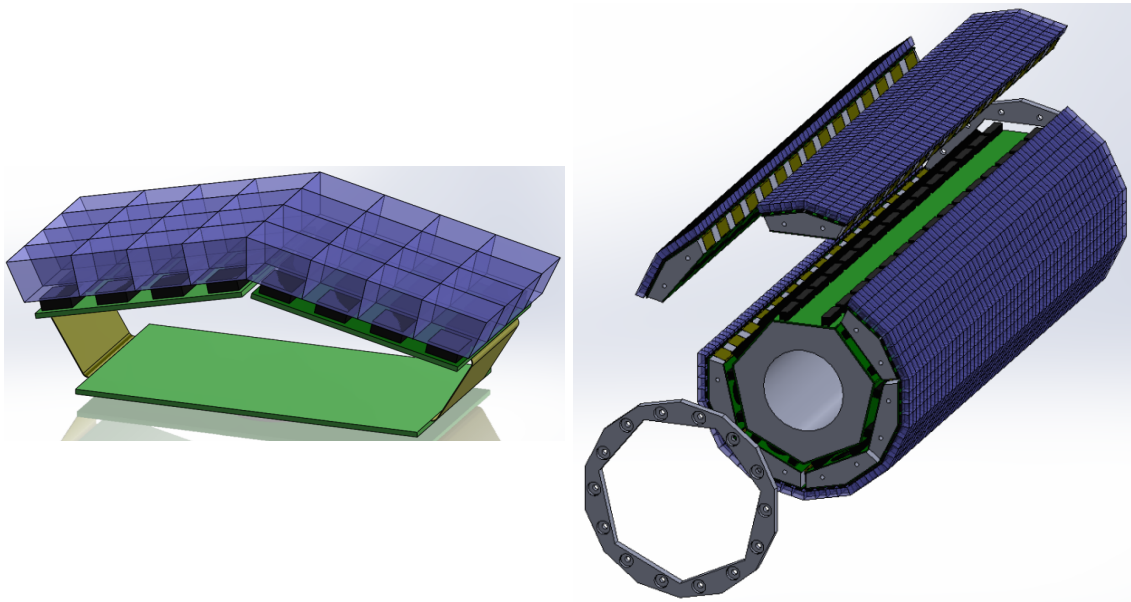


FIG. 6: *left*: submodule of the tile detector, *right*: explode view of a fully equipped detector station with seven modules [11]

Time of Flight System Readout

The baseline design uses the SiPM Timing Chip (STiC) [12] and a successor, the MuSTiC, that is a dedicated development for Mu3e. It will be used to read out the fibers and the tiles. The STiC chip is a mixed mode ASIC containing the analogue and digital part. For the analogue input two thresholds are used. The lower threshold specifies the timestamp of the input signal while the second threshold specifies the charge of the input signal by measuring the time over threshold. The intrinsic STiC time resolution has been measured being $\sigma_{\text{STiC}} < 30$ ps [13]. The STiC chip allows to vary the bias voltage within a window of 0.7 V. This allows to compensate the variations of the optimal SiPM bias voltage between different channels.

The STiC chip has been designed for a PET application with LYSO crystals where thousands of photons are expected. Also the tiles produce signals with ~ 1000 photons. Therefore the STiC chip can directly be used for the tile detector. For the fibers the STiC needs to operate with a few photons only. As SiPMs have high dark rates at low thresholds the main development for MuSTiC is to speed up the LVDS link to write out the data. The current design of the STiC and MuSTiC is not able to measure the time over threshold for signals containing a few photons only. Therefore additional R&D is needed to provide the feature for the fiber detector.

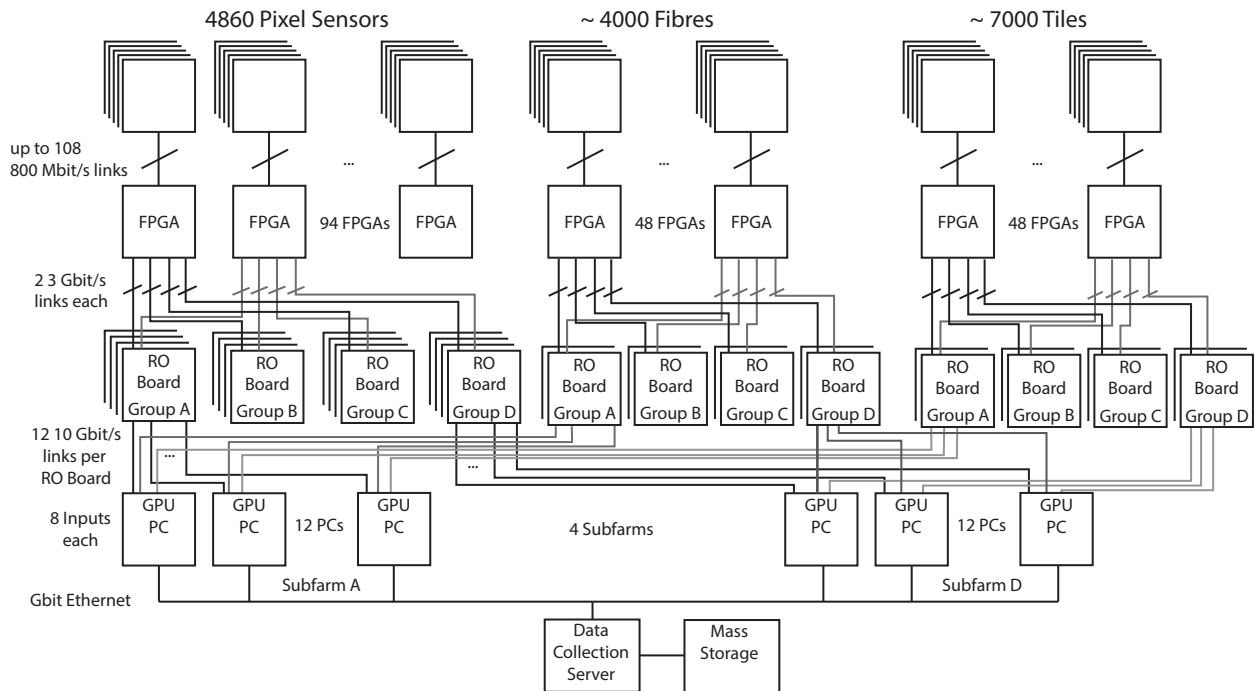


FIG. 7: Three staged readout scheme for Mu3e [14].

DATA ACQUISITION

The Mu3e experiment produces overall several Tbit s^{-1} of zero-suppressed data. Fig. 7 shows the readout of the experiment. The STiC chips from the tiles and fibers as the HV-MAPS pixel sensors provide digital differential LVDS links to the front-end FPGAs placed close to the detector. The front-end FPGAs merge and buffer data from the LVDS links and send them via optical links to the counting house. The optical links are not only needed to provide high enough bandwidth to transfer the data to the counting house but it also decouples the detector galvanically from the counting house electronics. The data is sent to the counting house by time slices to four different sub-farm FPGAs of the event filter farm in sequence. The sub-farm FPGAs are again connected to 12 computers for each sub-farm. In each computer a third FPGA rejects already tracks that are not coinciding in time. The rest of the data is sent to a graphics processing unit for reducing combinatorial background by reconstructing the muon vertex position. At the end the data written to tape will be reduced to less than 100 MB s^{-1} [14].

* Presented at NuFact15, 10-15 Aug 2015, Rio de Janeiro, Brazil [C15-08-10.2]

† rgredig@physik.uzh.ch; Speaker

‡ URL: <http://www.psi.ch/mu3e>

- [1] U. Bellgardt et al. (SINDRUM Collaboration), Nuclear Physics B **299**, 1 (1988).
- [2] Y. Fukuda et al. (Super-Kamiokande Collaboration), Phys. Rev. Lett. **81**, 1562 (1998).
- [3] Q. R. Ahmad et al. (SNO Collaboration), Physical Rev. Lett. **87**, 071301 (2001), 0106015.
- [4] K. Eguchi et al. (KamLAND Collaboration), Phys. Rev. Lett. **90**, 21802 (2002), 0212021.

- [5] A. Blondel et al., p. 104 (2013), 1301.6113.
- [6] M. L. Brooks et al. (MEGA Collaboration), *Phys. Rev. Lett.* **83**, 1521 (1999).
- [7] J. Adam et al. (MEG Collaboration), *Phys. Rev. Lett.* **110**, 201801 (2013).
- [8] W. Bertl et. al (SINDRUM II Collaboration), *European Physical Journal C* **47**, 337 (2006).
- [9] A. Herkert, Master's thesis, Heidelberg University (2015).
- [10] I. Perić, *Nucl. Instrum. Meth.* **582**, 876 (2007).
- [11] P. Eckert, Ph.D. thesis, Heidelberg University (2015).
- [12] T. Harion et al., *Journal of Instrumentation* **9**, C02003 (2014).
- [13] W. Shen et al., in *2013 IEEE Nuclear Science Symposium and Medical Imaging Conference (2013 NSS/MIC)* (IEEE, 2013), pp. 1–5.
- [14] D. Wiedner et al., *Journal of Instrumentation* **9**, C01011 (2014).